Rock and Soil Mechanics

Volume 44 | Issue 5 Article 1

8-21-2023

Mechanical properties of fractured sandstone after cyclic thermal shock

Man LI
Key Laboratory of New Technology for Construction of Cities in Mountain Area, Ministry of Education, Chongqing University, Chongqing, 400045, China, School of Civil Engineering, Chongqing University, Chongqing, 400045, China

Xian-shan LIU
Key Laboratory of New Technology for Construction of Cities in Mountain Area, Ministry of Education, Chongqing University, Chongqing, 400045, China, School of Civil Engineering, Chongqing University, Chongqing, 400045, China

Yu-hua PAN
School of Civil Engineering, Chongqing University, Chongqing, 400045, China

Shi-hao QIAO
School of Civil Engineering, Chongqing University, Chongqing, 400045, China

See next page for additional authors

Mechanical properties of fractured sandstone after cyclic thermal shock

Authors

Man LI, Xian-shan LIU, Yu-hua PAN, Shi-hao QIAO, Zi-yu HAO, Lei QIAN, and Xiao-lei LUO

Rock and Soil Mechanics 2023 44(5): 1260−1270 ISSN 1000−7598
https: //doi.org/10.16285/j.rsm.2022.5900 http://rocksoilmech.researchcommons.org/journal

Mechanical properties of fractured sandstone after cyclic thermal shock

LI Man[1, 2], LIU Xian-shan[1, 2], PAN Yu-hua[2], QIAO Shi-hao[2], HAO Zi-yu[2], QIAN Lei[2], LUO Xiao-lei[2]

1. Key Laboratory of New Technology for Construction of Cities in Mountain Area, Ministry of Education, Chongqing University, Chongqing, 400045, China
2. School of Civil Engineering, Chongqing University, Chongqing, 400045, China
3. National Joint Engineering Research Center of Geohazards Prevention in the Reservoir Areas, Chongqing University, Chongqing 400045, China

Abstract: The stimulation of thermal reservoirs in sandstone and its long-term stability evaluation are of great significance to the development of geothermal energy. In this paper, the mechanical properties of fractured sandstone under 0–8 cycles of thermal shocks are studied. The experimental results show that the P-wave velocity, uniaxial compressive strength (UCS) and elastic modulus of fractured sandstone all decrease gradually with the increase in the number of thermal shocks under two types of cooling methods. Compared with the cooling method in the water, the natural cooling method in the air causes less damage to the mechanical properties of fractured sandstone. The UCS and elastic modulus of fractured sandstone show a good exponential relationship with the number of thermal shocks. Both the P-wave velocity and elastic modulus can be used to describe the damage evolution of the fractured sandstone with the number of thermal shocks. The first thermal shock weakens the mechanical properties of fractured sandstone most severely, and the deterioration effect of mechanical properties is significantly reduced when the number of thermal shocks exceeds 4. In addition, the UCS and elastic modulus of fractured sandstone also have a good exponential relationship with the P-wave velocity. Finally, the thermal shock process of sandstone specimens is simulated in COMSOL Multiphysics, and the effects of the heat conductivity coefficient and prefabricated cracks on the internal temperature and stress fields of sandstone are discussed, revealing the mechanism of thermal cracking in sandstone under the effect of thermal shock.

Keywords: sandstone; prefabricated fissure; cyclic thermal shock; damage evolution; thermal cracking

1 Introduction

Social and economic development leads to rapid growth in the energy demand. To address energy supply challenges, the development and utilization of renewable energy becomes an important solution. As a clean, renewable and widely distributed energy source, geothermal energy has attracted much attention. In the process of geothermal energy production, low-temperature fluid is injected into the geothermal reservoir through injection wells. It can fully absorb the energy of the high-temperature matrix by heat convection in the fracture network[1–4]. When the cryogenic fluid is in contact with the geothermal reservoir, a significant temperature gradient will occur in the rock in a short time due to the effect of thermal shock, resulting in a large thermal stress. Once the thermal stress exceeds the strength of mineral particles, thermal cracks appear, which will affect the physico-mechanical properties of the geothermal reservoir and ultimately influence the production of geothermal energy[5–8]. The damage mechanism of thermal shock to rocks is different from the damage caused by nonuniform thermal expansion of mineral particles at high temperatures. In addition, the extraction of geothermal energy in enhanced geothermal systems (EGSs) is a long-term project that requires frequent water injection and extraction, thus it is important to study the physico-mechanical properties of geothermal reservoirs after multiple heating and cooling treatments.

In recent years, many researchers have studied the physico-mechanical properties of high-temperature rocks. For example, Zhao et al.[5] revealed the three-dimensional (3D) mesoscopic rupture mechanism of granite at 500 °C based on computed tomography (CT) technology. Zhao et al.[9] studied the variations in ultrasonic velocity and porosity of thermally treated sandstone specimens and discussed the relationship between ultrasonic velocity and thermal damage. Sun et al.[10] carried out the experiments on the physico-mechanical properties of granite after high-temperature treatment, studied the uniaxial compressive strength (UCS) and permeability of thermally treated granite, and verified the phase transition of quartz near 573 ℃. Kim et al.[11] conducted the mechanical tests on high-temperature rocks under rapid cooling and simulated the 3D distributions of temperature and stress fields under thermal shock using the ANSYS simulator. Zhu et al.[12] studied the physico-mechanical properties of granite at the temperatures below 500 ℃ and analyzed the physico-mechanical deterioration mechanism of high-temperature granite under hydrothermal shock from a microscopic perspective by scanning electron microscopy (SEM). Fan et al.[13] used CT scanning and image analysis to study the damage distribution of granite subjected to thermal shock at different temperatures. Hao et al.[14] carried out a thermal shock test on granite in the Qinghai Gonghe Basin at different

Received: 14 June 2022 Accepted: 18 September 2022
This work is supported by the National Natural Science Foundation of China (52279094) and the Key Research and Development Program of Guangxi (AB20238036).
First author: LI Man, male, born in 1994, PhD candidate, focusing on multi-field coupling in fractured rocks. E-mail：manli@cqu.edu.cn
Corresponding: LIU Xian-shan, female, born in 1978, PhD, Professor, research interests: geotechnical engineering seepage, multi-field coupling theory and numerical methods. E-mail：liuxianshan@163.com

cooling temperatures and analyzed the evolution of mechanical properties of granite with cooling water temperature. Yang et al.[15] studied the evolution of internal pores in sandstone at 600 ℃ after thermal shock cooling at different water temperatures and analyzed the relationship between the cooling temperature and pore fractal dimension. Although some progress has been made in the study of the physico-mechanical properties of rocks heated at high temperatures after rapid thermal shock, there are few studies on the mechanical properties of rocks, mainly for intact rocks after cyclic thermal shock. Zeng et al.[16] studied crack growth in fine-grained marble after high-temperature cycling and analyzed the influence of the number of thermal cycles on microcrack growth in marble by counting the length, aperture and number of cracks. Li et al.[17] analyzed the Brazilian splitting characteristics of granite and the evolution of wave velocity with the number of thermal cycles after cyclic cooling at different temperatures. It was found that the number of thermal cycles at medium and high temperatures (300–700 ℃) significantly deteriorated the tensile strength and wave velocity. Rong et al.[18] carried out the physico-mechanical tests on granite that was cooled by liquid nitrogen from 300 ℃. It was found that the damage to granite mainly occurred in the first few cycles of thermal shock. When the number of thermal cycles exceeded 12, the damage to granite almost no longer accumulated. However, the natural rock contains many micropores and cracks, making the study of the mechanical properties of fractured rock masses after cyclic thermal shock need to be supplemented.

Based on the above analysis, a series of cyclic thermal shock and uniaxial compression tests was performed on sandstone specimens with prefabricated cracks. The influence of the number of thermal shocks on the mechanical properties, including the damage to fractured sandstone under different cooling methods, was studied. Then, the thermal shock process of sandstone was simulated using the finite element method-based simulator COMSOL Multiphysics, and the effects of the convective heat transfer coefficient and prefabricated cracks on the distribution of internal temperature and stress fields of sandstone were discussed. The results can provide effective support for the reconstruction and long-term reliability analysis of geothermal reservoirs.

2 Experimental principle and schemes

2.1 Specimen preparation

The gray-white sandstone specimens with a density of 2 450 kg/m^3 were taken from the tight sandstone reservoir in Jiulongpo District, Chongqing, China. X-ray diffraction (XRD) test was used to analyze the components. From the diffraction pattern, it can be seen that sandstone is mainly composed of 41.90% quartz, 24.92% feldspar, 10.82% calcite and 22.36% clay minerals, as shown in Fig. 1. According to the recommended method of the International Society for Rock Mechanics (ISRM)[19], the sandstone was processed into standard cylindrical specimens with a height of 100 mm and a diameter of 50 mm after drilling, cutting and polishing. To obtain the fractured sandstone, a crack with an inclination of 45° (i.e. maximum shear stress direction), a length of 12 mm, and a width of 1.5 mm was fabricated in the middle of a standard cylindrical specimen using waterjet cutting technology, as shown in Fig. 2.

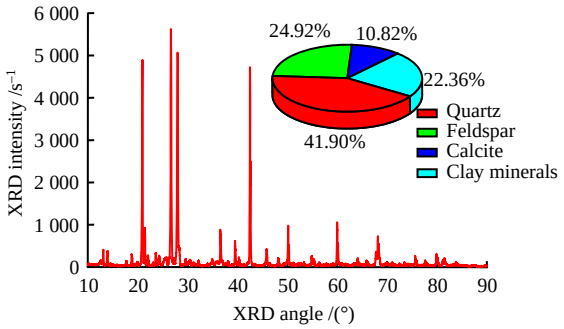

Fig. 1 XRD analysis of sandstone

(a) Sandstone specimen with prefabricated crack

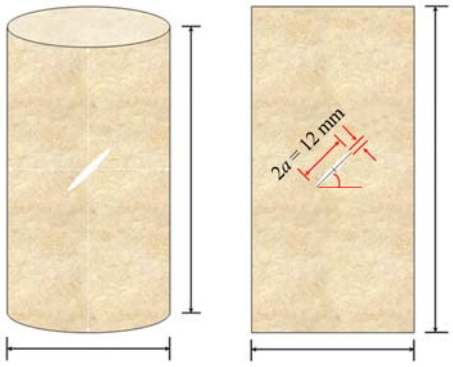

(b) Geometry of the crack in the specimen

Fig. 2 Fractured sandstone specimens

2.2 Test equipment

A nonmetallic ultrasonic detector was used to detect the P-wave velocity of fractured sandstone specimens that were separately cooled in the air and water for different thermal shocks. The sandstone specimen was heated in a 3 kW muffle furnace with a maximum heating temperature of 1 100 ℃ and a temperature error of ±5 ℃. In addition, to reduce the safety risk in the high-temperature environment and accurately measure the temperatures of sandstone specimens and the cooling water during the thermal shock process, a noncontact infrared thermometer AS700 (accuracy within 2%) was used to measure the

temperature in real time. The uniaxial compression test was performed on a microcomputer-controlled electrohydraulic servo rock shear rheological testing machine WADJ-600 with a maximum axial load of 600 kN and a maximum axial displacement of 30 mm. All the test devices used in the experiment are shown in Fig. 3.

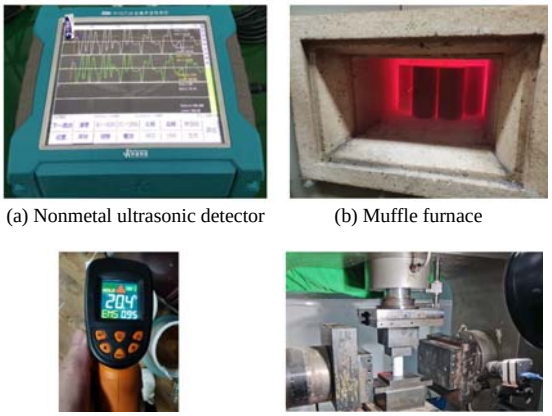

(a) Nonmetal ultrasonic detector (b) Muffle furnace

(c) Infrared thermometer AS700 (d) Shear rheological machine WADJ-600

Fig. 3 Test devices

2.3 Experimental procedure

To study the mechanical properties of fractured sandstone under cyclic thermal shock, the fractured sandstone specimen was subjected to multiple cyclic heating and cooling treatments, and then a uniaxial compression test was carried out. The specific experimental procedure is described as follows:

(1) Thermal treatment test: It is shown that the deterioration of the mechanical properties of the rock by cyclic thermal treatment is weak when the temperature is too low. The deterioration of the physico-mechanical properties of the rock is obvious at medium and high temperatures (> 300 ℃)[17]. In addition, when the temperature is very high, some minerals in the sandstone undergo physico-chemical reactions during heating. For example, the phase change of quartz in the sandstone occurs at 573 ℃, and calcite will decompose at 700–830 ℃, which will have an impact on the experimental results. In this study, 400 ℃ was selected as the target temperature for the thermal shock of reservoir sandstone. All the sandstone specimens were heated to 400 ℃ in a muffle furnace at a heating rate of 5 ℃/min. The target temperature was maintained for 2 h to fully heat the sandstone specimens to reduce the influence of the internal temperature gradient of the sandstone on thermal shock[8].

(2) Thermal shock test: The heated sandstone specimens were removed from the muffle furnace for the subsequent thermal shock test. Before the thermal shock test, sufficient distilled water should be prepared in advance, and the water temperature should be strictly controlled by the infrared thermometer AS700, making the complete thermal shock process of sandstone at the target water temperature. After the specimen was completely cooled in the water, it was removed from the water, and the dryer was used to remove the remaining moisture inside the sandstone. Heat treatment and thermal shock tests were repeated, and the number of thermal shocks was set to 0, 1, 4 and 8. When the number of thermal shocks is 0, it is indicated that the sandstone is in the natural state (unheated), and air cooling is also set for comparison. The sandstone specimens are named as follows: for example, in "W-1", "W" represents water cooling, and "1" means that the number of thermal cycles is 1. In addition, "A" stands for air cooling, and the cooling temperatures of the air and water are 20 °C during the test. The test conditions of sandstone specimens under different thermal shocks are listed in Table 1, and the cyclic thermal shock process is shown in Fig. 4.

(3) Uniaxial compression test: The uniaxial compression test of fractured sandstone was carried out on a microcomputer-controlled electrohydraulic servo rock shear rheological testing machine WADJ-600. The axial stress was loaded by the displacement-controlled method, and the loading rate was 0.1 mm/min. Three specimens were tested for each working condition to obtain the average value.

Table 1 Experimental conditions for thermal shock of fractured sandstone specimens

No.	Cooling method	Number of thermal shocks	Temperature of cooling medium /℃
A/W-0	Air/Water	0	20
A-1	Air	1	20
A-4	Air	4	20
A-8	Air	8	20
W-1	Water	1	20
W-4	Water	4	20
W-8	Water	8	20

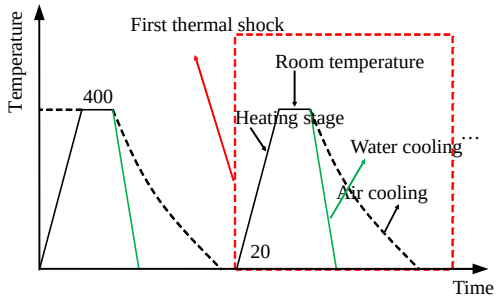

Fig. 4 Cyclic thermal shock process of sandstone

3 Experimental results and analysis

3.1 P-wave velocity of fractured sandstone

Figure 5 shows the variation curves of the P-wave velocity with the number of thermal shocks under different cooling methods. In general, with the increase in the number of thermal shocks, the P-wave velocity of sandstone specimens gradually decreases. Compared with the natural sandstone (number of thermal shocks =0), the P-wave velocities of sandstone specimens decrease by 3.54%, 5.17% and 7.55% when it is cooled in the air for 1, 4 and 8 times, respectively. Similarly, the P-wave velocities decrease by 11.56%, 27.42% and 33.21% when it is cooled in the water for

1, 4 and 8 times, respectively. This is due to the gradual increase in thermal cracks in the sandstone as the number of thermal shocks increases (Fig. 6). The presence of cracks hinders the propagation of sound wave in the sandstone, resulting in a decrease in the P-wave velocity of the sandstone specimen[20–21]. In addition, it can be seen from the results that the P-wave velocity attenuation of sandstone specimens is slightly affected by thermal shock in the air. With the increase in the number of thermal shocks in the air, the sensitivity of the P-wave velocity of sandstone specimens to thermal shock decreases, and the decrease in P-wave velocity is mainly concentrated in the first thermal shock. However, when the sandstone specimen is rapidly cooled by water, the effect of thermal shock is more significant due to the large convective heat transfer coefficient of liquid water, leading to an increase in the number of thermal cracks. Therefore, the attenuation of the P-wave velocity is more apparent. The test results of the P-wave velocity V_p are tabulated in Table 2.

3.2 Complete stress–strain curve of uniaxial compression test

The complete stress–strain curve of fractured sandstone under uniaxial compression is mainly divided into five stages[22–23]: (1) the compaction stage: micropores and microcracks in the sandstone are compressed greatly; (2) linear elastic stage: the stress–strain curve is approximately a straight line; (3) crack initiation and stable propagation stage: crack initiation and propagation occur and the stress–strain curve becomes nonlinear; (4) crack unstable propagation stage: the strain energy stored in the fractured sandstone is sufficient to rapidly create new cracks and maintain the rapid growth of existing microcracks; and (5) postpeak stress softening stage: when it exceeds the peak stress, the stress drops rapidly, as shown in Fig. 7. The compaction stage becomes longer, and the slope of the linear elastic stage gradually decreases with increasing number of thermal shocks. This is because more thermal cracks appear in the fractured sandstone with the increase in the number of thermal shocks, as shown in Fig. 6. The increase in the number of thermal cracks weakens the mechanical properties of fractured sandstone, and multiple local failures occur at the subsequent loading stages and finally reach peak stress. With the increase in the number

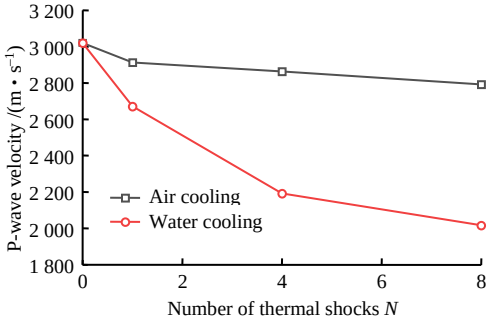

Fig. 5 Variations of P-wave velocity with the number of thermal shocks

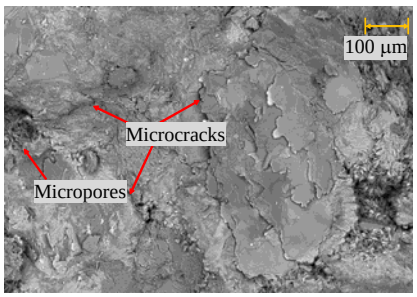

(a) After 1 thermal shock

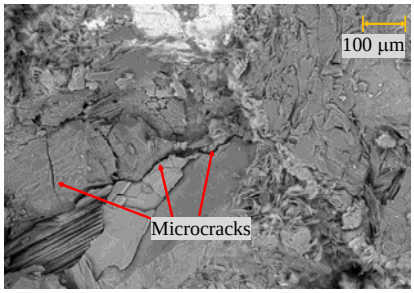

(b) After 4 thermal shocks

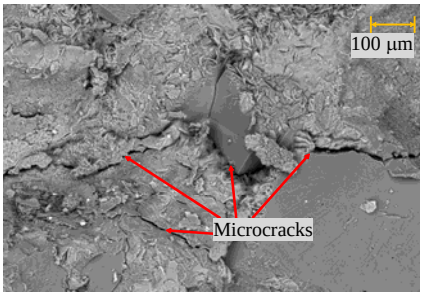

(c) After 8 thermal shocks

Fig. 6 Microstructures of sandstone specimens after cyclic thermal shocks (water at 20 °C)

Table 2 Values of P-wave velocity V_p, UCS and elastic modulus E under different testing conditions

No.	V_p /(m • s^{-1})	Average value of V_p /(m • s^{-1})	UCS /MPa	Average value of UCS /MPa	E /GPa	Average value of E /GPa
A/W-0-a	3 047		69.73		7.53	
A/W-0-b	3 003	3 020	60.34	64.76	7.21	7.39
A/W-0-c	3 010		64.21		7.43	
A-1-a	2 952		58.12		5.63	
A-1-b	2 901	2 913	56.12	54.63	5.41	5.02
A-1-c	2 886		49.65		4.02	
A-4-a	2 881		50.90		4.50	
A-4-b	2 773	2 864	48.37	50.47	4.21	4.58
A-4-c	2 938		52.14		5.03	
A-8-a	2 713		46.16		4.31	
A-8-b	2 812	2 792	48.70	48.75	4.49	4.45
A-8-c	2 851		51.39		4.55	
W-1-a	2 676		45.20		4.06	
W-1-b	2 710	2 671	46.71	44.70	4.76	4.11
W-1-c	2 627		42.19		3.51	
W-4-a	2 293		35.16		2.92	
W-4-b	2 341	2 192	37.15	35.18	3.43	3.02
W-4-c	1 942		33.23		2.71	
W-8-a	2 043		34.37		2.86	
W-8-b	2 031	2 017	33.64	33.34	2.94	2.80
W-8-c	1 978		32.02		2.61	

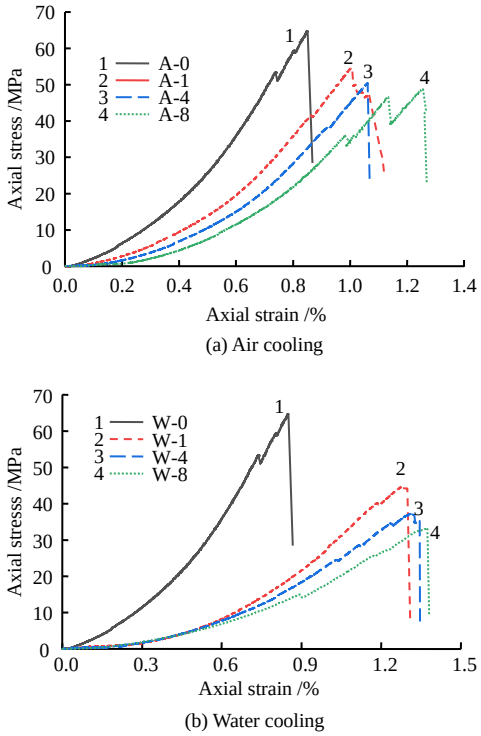

Fig. 7 Complete stress–strain curves of fractured sandstone under different numbers of thermal shocks

of thermal shocks, the peak stress gradually decreases, and the corresponding peak strain gradually increases. This is due to the gradual transformation from brittle to ductile in the fractured sandstone with the increase in the number of thermal shocks.

3.3 Uniaxial compressive strength and elastic modulus of fractured sandstone

UCS and elastic modulus are two important parameters reflecting the bearing capacity and deformation resistance of rocks, and different thermal shock methods may have significant impacts on both parameters. Figure 8 shows the variation curves of the UCS, elastic modulus and number of thermal shocks of fractured sandstone under different cooling methods. Figure 8 shows that the UCS and elastic modulus gradually decrease and eventually tend to be constant with the increase in the number of thermal shocks. The deterioration effect of the UCS and elastic modulus due to thermal shock in the water is more significant than that of thermal shock in the air. The exponential function is introduced to characterize the changes in UCS and elastic modulus with the number of thermal shocks[18, 24]. The results show that they have a good correlation with the number of thermal shocks. Compared with the final state, after the first thermal shock, the UCS and elastic modulus are decreased by 63.27% and 80.61%, respectively, under air cooling conditions, while they are decreased by 63.84% and 71.51%, respectively, under water cooling conditions. After the fourth thermal shock, the UCS and elastic modulus of the fractured sandstone under air cooling conditions are decreased by 89.26% and 95.58%, respectively, while they are decreased by 94.14% and 95.28%, respectively, under water cooling conditions. This indicates that the UCS and elastic modulus are the most sensitive parameters to the first thermal shock under different types of cooling conditions. When the number of thermal shocks exceeds 4, both the UCS and elastic modulus tend to be constant, and the influence of the number of thermal shocks on them is not obvious.

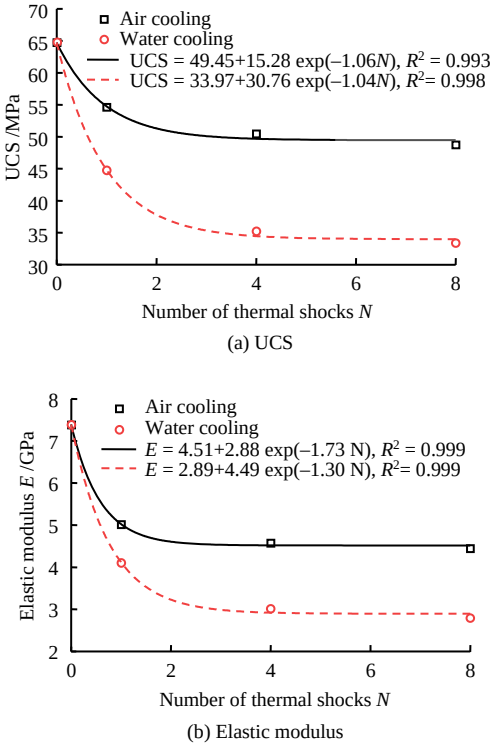

Fig. 8 Variations in UCS and elastic modulus with the number of thermal shocks

4 Discussion

4.1 Fractured sandstone damage under thermal shocks

During the thermal shock process, there is a significant temperature gradient in the sandstone, which results in a large thermal stress. When the thermal stress exceeds the tensile strength of mineral particles, the damage occurs in rocks. In addition, with the increase in the number of thermal shocks, the cracks in the sandstone further appear and propagate, resulting in damage accumulation, as shown in Fig. 9. To quantitatively characterize the damage to fractured sandstone with different numbers of thermal shocks, the elastic modulus and P-wave velocity are selected as the benchmarks to define the damage variables[9, 25].

$$D_{\mathrm{E}} = 1 - \frac{E_{\mathrm{T}}}{E_0} \tag{1}$$

$$D_{\mathrm{p}} = 1 - \left(\frac{V_{\mathrm{p2}}}{V_{\mathrm{p1}}}\right)^2 \tag{2}$$

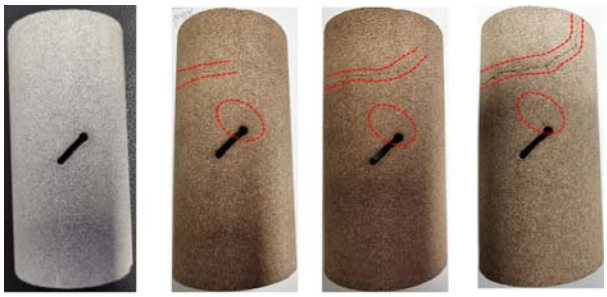

(a) N=0 (b) N=1 (c) N=4 (d) N=8

Fig. 9 Propagation of thermal cracks in fractured sandstone with the number of thermal shocks (water at 20 ℃)

where D_E is the damage variable based on the elastic modulus; E_T and E_0 are the elastic moduli of fractured sandstone before and after thermal shock, respectively; D_p is the damage variable based on the P-wave velocity; and V_{p1} and V_{p2} are the P-wave velocities of fractured sandstone before and after thermal shock.

Figure 10 shows the variation curves of damage variables of fractured sandstone with the number of thermal shocks under different cooling methods. Both the damage variables gradually accumulate and eventually become stable with increasing thermal shock. Under different cooling methods, the damage variables and the number of thermal shocks show a good exponential function. In addition, because the convective heat transfer coefficient of air is much smaller than that of water, the thermal shock strength in air cooling conditions for fractured sandstone is relatively weak, thus the damage to sandstone is less[26]. The elastic modulus is taken as an example. During the first thermal shock, the damage to sandstone under air and water cooling accounts for 80.61% and 71.51% of the total damage, respectively. During the fourth thermal shock, the damage to sandstone under air and water cooling accounts for 95.58% and 95.28% of the total damage, respectively. The accumulation of damage to sandstone is weak with the increase in the number of thermal shocks. This is because the cementation between the sandstone mineral particles is destroyed under the action of thermal stress at the beginning of thermal cycles, resulting in intergranular cracks and transgranular cracks. As the number of thermal cycles increases, the microcracks generated by previous thermal cycles have provided enough space for thermal expansion of mineral particles, thereby reducing thermal stress in the sandstone[18]. Therefore, after the number of thermal cycles reaches the threshold, the mechanical properties of sandstone hardly change, which is consistent with the variations in the P-wave velocity, UCS and elastic modulus.

4.2 Correlation between P-wave velocity and mechanical properties

The above results show that both the P-wave velocity and mechanical properties of sandstone present a decreasing trend with increasing number of thermal shocks, and there may be a certain correlation between both parameters[27]. When the rock is affected by thermal shock, the microcracks appear, and the wave velocity is more sensitive to the variation in cracks, which can indirectly reflect the damage to rocks to predict the mechanical properties of the rock. Figure 11 shows the relationships of the UCS and elastic modulus of fractured sandstone with the P-wave velocity. The UCS and elastic modulus have a satisfactory exponential relationship with the P-wave velocity. The measurement of the P-wave velocity of rocks is not as cumbersome

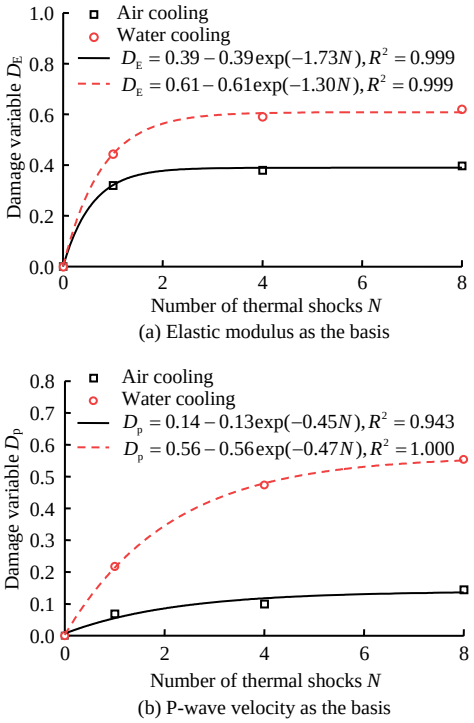

Fig. 10 Variations of damage variables with the number of thermal shocks

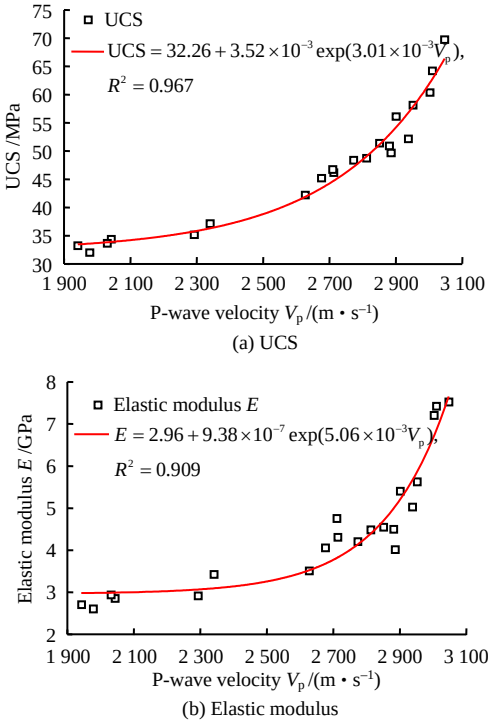

Fig. 11 Relationships of UCS and elastic modulus of fractured sandstone with P-wave velocity

and costly as the UCS, and other mechanical properties of rocks. The correlation between the P-wave velocity and mechanical parameters can provide a simple and effective method for predicting the mechanical properties of deep sandstone geothermal reservoirs.

4.3 Effect of convective heat transfer coefficient on thermal shock

It can be concluded from previous studies[28–30] that the main factors inducing thermal damage to rocks during thermal shock include the temperature of rocks and the cooling medium or the temperature difference between the rock and the cooling medium. In addition, the convective heat transfer coefficient during thermal shock is also a key parameter, thus the factors related to the convective heat transfer coefficient also affect the thermal damage to rock, such as the type of cooling medium, flow rate and contact area between the rock surface and the cooling fluid. This paper discusses the effects of the convective heat transfer coefficient and prefabricated cracks on thermal shock by numerical analysis.

There are significant differences in the physico-mechanical properties of fractured sandstone after cooling in the air and liquid water, which are mainly affected by the difference in the convective heat transfer coefficient during thermal shock. The influence of the convective heat transfer coefficient on the temperature and stress of sandstone under different cooling methods is studied numerically. In this study, only the temperature and stress distributions of fractured sandstone specimens under the first thermal shock are discussed, and the influence of rock heterogeneity on thermal shock is ignored. The cooling of fractured sandstone specimens in the air is a natural convection state, while the cooling in water is a strong convection state. We select the air and water at 20 ℃ as the cooling medium in the simulation, and the corresponding convective heat transfer coefficients are set as 20 and 2 000 W/(m^2·K). Other physico-mechanical parameters are listed in Table 3. A fractured sandstone model is established in the commercial finite element software COMSOL Multiphysics 5.6, as shown in Fig. 12.

Table 3 Physico-mechanical parameters of sandstone input into numerical simulation

Elastic modulus /GPa	Poisson's ratio	Density /(kg • m^{-3})	Coefficient of thermal expansion /(K^{-1})	Heat conductivity coefficient /(W • m^{-1} • K^{-1})	Specific heat capacity /(J • kg^{-1} • K^{-1})	Tensile strength /MPa
7.39	0.25	2 450	5.4×10^{-6}	3.0	880	5.82

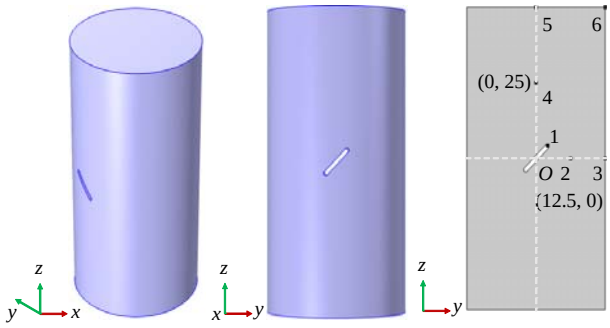

(a) 3D model (b) *yoz* view (c) Two-dimensional model

Fig. 12 Numerical models of fractured sandstone

The thermo-mechanical coupling equation of rocks can be written as

$$\left.\begin{aligned}&\nabla\cdot\boldsymbol{\sigma}+\boldsymbol{F}_{\mathrm{v}}=\rho\ddot{\boldsymbol{u}}\\&\boldsymbol{\varepsilon}=\frac{1}{2}\left[(\nabla\boldsymbol{u})^{\mathrm{T}}+\nabla\boldsymbol{u}\right]\\&\boldsymbol{\sigma}=\boldsymbol{C}(E,\mu):(\boldsymbol{\varepsilon}-\boldsymbol{\varepsilon}_{\mathrm{th}})\end{aligned}\right\}\tag{3}$$

where $\boldsymbol{\sigma}$ is the Cauchy stress tensor; $\boldsymbol{F}_{\mathrm{v}}$ is the volumetric force vector; ρ is the rock density; $\boldsymbol{u}$ is the displacement; $\ddot{\boldsymbol{u}}=\partial^2\boldsymbol{u}/\partial t^2$ is the 2nd derivative of displacement versus time; $\boldsymbol{\varepsilon}$ is the total strain; $\boldsymbol{C}(E,\mu)$ is the fourth-order stiffness matrix related to the elastic modulus of the material and the Poisson's ratio; and $\boldsymbol{\varepsilon}_{\mathrm{th}}$ is the thermal expansion strain.

The heat transfer equation is

$$\rho C_{\mathrm{p}}\frac{\partial T}{\partial t}+k\nabla^2T=Q\tag{4}$$

where C_{p} is the specific heat capacity; k is the thermal conductivity; Q is the source item; and T is the temperature.

The convective boundary conditions are introduced to characterize the thermal shock of rocks:

$$q_0=h(T_{\mathrm{ext}}-T)\tag{5}$$

where q_0 is the boundary heat flux; h is the convective heat transfer coefficient; and T_{ext} is the external temperature of the system. The convective boundary conditions are set on the outer surface of fractured sandstone and prefabricated crack surfaces.

Six monitoring points are selected to record the variations in internal temperature and maximum principal stress over time. Figure 13 shows that the temperature at the six monitoring points slowly decreases with time after air cooling. The effect of thermal shock is relatively moderate due to the small convective heat transfer coefficient. The maximum temperature difference between monitoring points Nos. 4 and 6 is 54.16 ℃ at 266 s, and the final average temperature of the sandstone after 9000 s (i.e. 2.5 h) of thermal shock is approximately 21.5 ℃. The total cooling time is basically the same as that of natural cooling of sandstone specimens. After the water cooling, due to the influence of strong convection, the temperature at some monitoring points, including points Nos. 3, 5 and 6 at the outermost of the sandstone specimen and the monitoring point No. 1 at the internal crack tip that are in direct contact with the water, drops sharply at the moment of thermal shock. For the monitoring points Nos. 2 and 4 that are located in the sandstone specimen, the effect of thermal shock is relatively moderate, and the temperature difference between the monitoring point Nos. 4 and 6 reaches a maximum of 370.3 ℃ at 21 s, indicating that there is

a significant temperature gradient in the sandstone, resulting in a large thermal stress.

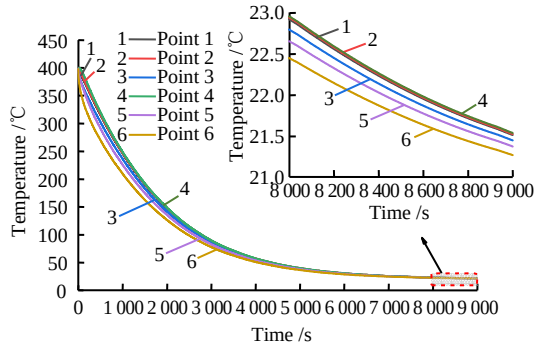

(a) Air cooling

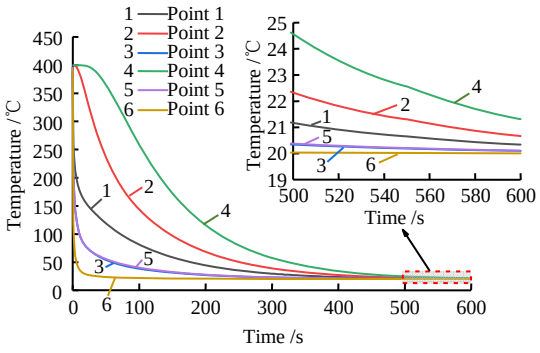

(b) Water cooling

Fig. 13 Variations of temperature at monitoring points with time under different types of cooling methods

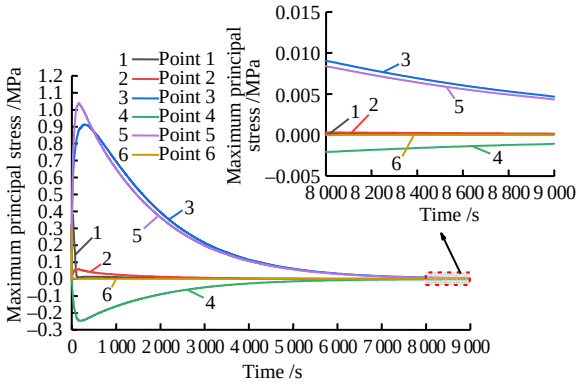

(a) Air cooling

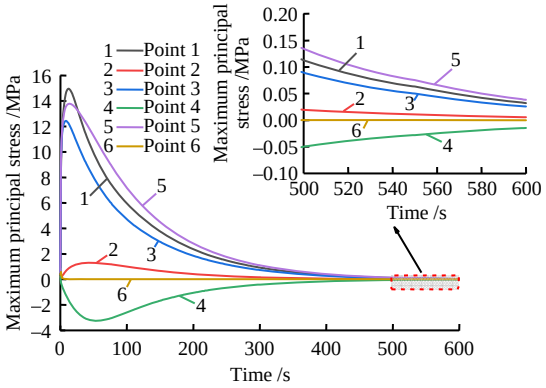

(b) Water cooling

Fig. 14 Variations of maximum principal stress at monitoring points with time under different types of cooling methods

As a typical brittle material, most of the thermal fracture of rocks belongs to tensile failure. In this study, the maximum tensile stress criterion is used to judge the damage to fractured sandstone under thermal stress. The tensile strength of sandstone obtained by the Brazilian splitting test is 5.82 MPa. Figure 14 shows the curves of the maximum principal stress at the internal monitoring point of the sandstone with time, assuming that the tensile stress is positive and the compressive stress is negative. After air cooling, the internal temperature gradient of the sandstone specimen is not very large due to the relatively moderate thermal shock effect. The maximum value of the maximum principal stress at the six monitoring points during the thermal shock process is 2.17 MPa, which is less than the tensile strength of sandstone. Therefore, no macroscopic cracks appear on the surface. After water cooling, large tensile stresses occur at monitoring points Nos. 1, 3 and 5 at the early stage of thermal shock, and then they gradually decrease to 0. For both air cooling and water cooling, only monitoring point No. 4 is in the compressive state among the six monitoring points, while monitoring point No. 6 is in the weak tensile stress state at the moment of thermal shock, and the stress at the subsequent stage is 0.

To illustrate the temperature and stress of sandstone under thermal shock, the ratio of the damage area S_D to the total area S_0 is selected. The damage area is obtained by integrating the maximum principal stress beyond the tensile strength in the fractured sandstone, and the ratio of the damage area to the total area with time in the fractured sandstone is shown in Fig. 15. The damage area of the fractured sandstone specimens is the largest at 23 s, and its temperature field is shown in Figs. 16(a)–16(c). The internal temperature gradient of the fractured sandstone reaches a maximum of 84 ℃/mm at the tip of the prefabricated fracture in both the *Y* and *Z* directions. In addition, the significant temperature gradients in the middle of the respective directions cause large thermal stresses (Fig. 16(d)). The thermal cracks can occur once the thermal stress exceeds the tensile strength. Figure 16(e) shows the damage distribution area of fractured sandstone, which is basically consistent with the location of the crack in the test (Fig. 9).

4.4 Effect of prefabricated cracks on thermal shock

It can be seen from the tests that the variation in the mechanical properties of fractured sandstone is basically the same as that of intact rocks with the number of thermal shocks. Their mechanical properties gradually deteriorate with the increase in the number of thermal shocks. The mechanical properties tend to be stable when the number of thermal shocks reaches

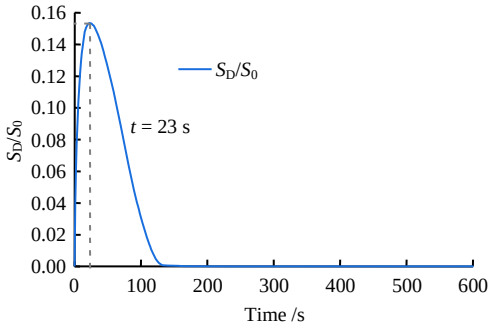

Fig. 15 Ratio of damage area to total area of sandstone as a function of time

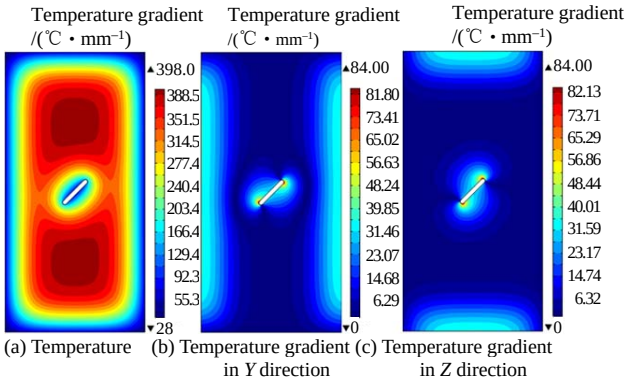

Fig. 16 Distributions of temperature and stress fields of fractured sandstone after water cooling at 23 s

the threshold[18, 21]. To study the influence of prefabricated cracks on the thermal shock process, the numerical simulation methods are used to study the thermal shock process of intact sandstone, and the numerical results are compared with the laboratory test results of fractured sandstone. The physico-mechanical parameters of intact sandstone are consistent with those of fractured sandstone, as listed in Table 3. The water at 20 ℃ is selected as the cooling medium for thermal shock, i.e. the convective heat transfer coefficient is 2 000 W/(m^2 • K). To control the variables, the distributions of temperature and stress in intact sandstone after thermal shock at 23 s are also selected, as shown in Fig. 17.

Figures 17(a)–17(c) show the temperature and stress variations when the high-temperature rock is in contact with low-temperature water during the thermal shock. Compared with the fractured sandstone, the low-temperature region diffuses from the outside to the inside of the intact sandstone. The maximum value of the temperature gradient occurs in the middle of the Y and Z directions, resulting in significant thermal stresses, which eventually leads to thermal damage. The integral method is used to obtain the damage area of intact sandstone. The damage area of intact sandstone is 1.08 times that of fractured sandstone. Although the existence of prefabricated cracks increases the contact area between sandstone and water, in some areas between prefabricated cracks and the outer surface, the thermal stress caused by the interaction between internal and external thermal shock inhibits each other, thereby reducing the stress distribution in this area so that the damage area of fractured sandstone is smaller than that of intact sandstone. Among them, the presence of cracks has little effect on the distribution of damage area in the Z direction (height direction). However, it can be observed that the prefabricated crack has an inhibitory effect on the damage area in the Y direction (radial direction), which can be attributed to the size effect of the specimen. The above phenomena show that in the process of oil and gas exploitation with thermal stimulation technology to increase the reservoir permeability, the contact area between the rock and the cooling medium is not the larger the better, but the locations of natural cracks in the reservoir should be comprehensively considered.

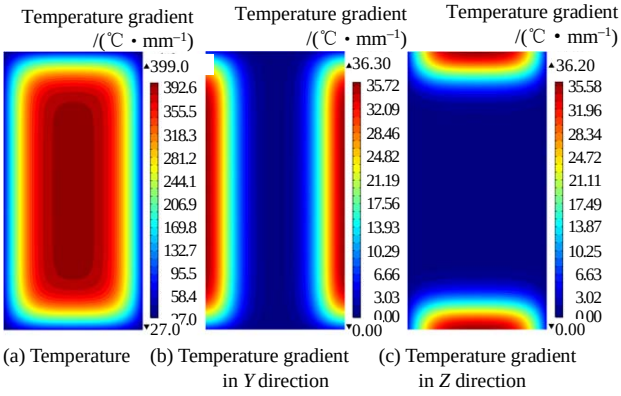

Fig. 17 Distributions of temperature and stress fields of intact sandstone after water cooling at 23 s

5 Conclusions

A series of cyclic thermal shock and uniaxial compression tests on fractured sandstone was carried out to study the mechanical properties of fractured sandstone under different numbers of thermal shocks.

Subsequently, the thermal shock process of sandstone was simulated in COMSOL Multiphysics. The distributions of temperature and stress in fractured sandstone were analyzed. The main conclusions are drawn as follows:

(1) The UCS and elastic modulus of fractured sandstone decrease with increasing number of thermal shocks, presenting a good exponential relationship. Among them, the first thermal shock results in the most serious deterioration of the mechanical properties of fractured sandstone. When the number of thermal shocks exceeds 4, the deterioration effect is significantly slowed down. Compared with water cooling, air cooling has a much weaker deterioration effect on the physico-mechanical properties of fractured sandstone.

(2) Both the P-wave velocity and elastic modulus can better characterize the damage to fractured sandstone. With the increase in the number of thermal shocks, both damage variables gradually accumulate and eventually stabilize. This is because the cementation between the sandstone mineral particles is destroyed due to thermal stress during the first few thermal shocks, resulting in intergranular cracks and transcrystalline cracks. As the number of thermal shocks increases, the cracks generated by the previous thermal shocks have provided enough space for thermal expansion of mineral particles, thereby reducing the thermal stress in the sandstone.

(3) During the thermal shock process, the largest temperature gradient appears at the tip of the prefabricated fracture in both the *Y* and *Z* directions of the fractured sandstone. In addition, a significant temperature gradient occurs in the middle of the radial and axial directions, which will lead to large thermal stresses. The thermal cracks appear once the thermal stress exceeds the tensile strength, which is basically the same as the location of the prefabricated crack in the test.

(4) The existence of prefabricated cracks increases the contact area between sandstone and water. Due to the interaction between internal and external thermal shocks, the thermal stresses inhibit each other in some parts of the area between prefabricated cracks and the outer surface, reducing the stress distribution in this area so that the damage area of fractured sandstone is smaller than that of intact sandstone.

References

[1] XU Tian-fu, ZHANG Yan-jun, ZENG Zhao-fa, et al. Technology progress in an enhanced geothermal system (hot dry rock)[J]. Science and Technology Review, 2012, 30(32): 42–45.

[2] PANG Zhong-he, LUO Ji, CHENG Yuan-zhi, et al. Evaluation of geological conditions for the development of deep geothermal energy in China[J]. Earth Science Frontiers, 2020, 27(1): 134–151.

[3] YU Li, PENG Hai-wang, LI Guo-wei, et al. Experimental study on granite under high temperature-water cooling cycle[J]. Rock and Soil Mechanics, 2021, 42(4): 1025–1035.

[4] XUE Hui, SHU Biao, CHEN Jun-jie, et al. Experimental study on mechanical properties of granite after reaction with $ScCO_2$ at high temperature and high pressure[J]. Rock and Soil Mechanics, 2022, 43(2): 377–384.

[5] ZHAO Yang-sheng, MENG Qiao-rong, KANG Tian-he, et al. Micro-CT experimental technology and meso-investigation on thermal fracturing characteristics of granite[J]. Chinese Journal of Rock Mechanics and Engineering, 2008, 27(1): 28–34.

[6] YANG S Q, RANJITH P G, JING H W, et al. An experimental investigation on thermal damage and failure mechanical behavior of granite after exposure to different high temperature treatments[J]. Geothermics, 2017, 65: 180–197.

[7] ZHAO Yi-qing, WU Chang-gui, JIN Ai-bing, et al. Experimental study on microstructure and mechanical properties of sandstone after heat treatment at high temperature[J]. Rock and Soil Mechanics, 2020, 41(7): 2233-2240.

[8] LI M, LIU X S. Effect of thermal treatment on the physical and mechanical properties of sandstone: insights from experiments and simulations[J]. Rock Mechanics and Rock Engineering, 2022, 55(6): 3171–3194.

[9] ZHAO Hong-bao, YIN Guang-zhi, CHEN Lun-jian. Experimental study on effect of temperature on sandstone damage[J]. Chinese Journal of Rock Mechanics and Engineering, 2009, 28(Suppl.1): 2784–2788.

[10] SUN Qiang, ZHANG Zhi-zhen, XUE Lei, et al. Physico-mechanical properties variation of rock with phase transformation under high temperature[J]. Chinese Journal of Rock Mechanics and Engineering, 2013, 32(5): 935–942.

[11] KIM K, KEMENY J, NICKERSON M. Effect of rapid thermal cooling on mechanical rock properties[J]. Rock Mechanics and Rock Engineering, 2013, 47(6): 2005–2019.

[12] ZHU Zhen-nan, TIAN Hong, DONG Nan-nan, et al. Experimental study of physico-mechanical properties of heat-treated granite by water cooling[J]. Rock and Soil Mechanics, 2018, 39(Suppl.2): 169–176.

[13] FAN L, GAO J, DU X, et al. Spatial gradient distributions of thermal shock-induced damage to granite[J]. Journal of Rock Mechanics and Geotechnical Engineering, 2020, 12(5): 917–926.

[14] XI Bao-ping, WU Yang-chun, ZHAO Yang-sheng, et al. Experimental investigations of compressive strength and thermal damage capacity characterization of granite under different cooling modes[J]. Chinese Journal of Rock Mechanics and Engineering, 2020, 39(2): 286–300.

[15] YANG Xin-xin, XI Bao-ping, HE Shui-xin, et al. Analysis of fracture characteristics and pore connectivity of sandstone under thermal shock[J]. Chinese Journal of Geotechnical Engineering, 2022, 44(10): 1925–1934.

[16] ZENG Yan-jin, RONG Guan, PENG Jun, et al. Experimental study of crack propagation of marble after high temperature cycling[J]. Rock and Soil Mechanics, 2018, 39(Suppl.1): 220–226.

[17] LI Chun, HU Yao-qing, ZHANG Chun-wang, et al. Brazilian split characteristics and mechanical property evolution of granite after cyclic cooling at different

temperatures[J]. Chinese Journal of Rock Mechanics and Engineering, 2020, 39(9): 1797–1807.

[18] RONG G, SHA S, LI B, et al. Experimental investigation on physical and mechanical properties of granite subjected to cyclic heating and liquid nitrogen cooling[J]. Rock Mechanics and Rock Engineering, 2021, 54(5): 2383–2403.

[19] FAIRHURST C E, HUDSON J A. Draft ISRM suggested method for the complete stress-strain curve for intact rock in uniaxial compression[J]. International Journal of Rock Mechanics and Mining Sciences, 1999, 36(3): 281–289.

[20] WU Zhi-sheng, FENG Zi-jun, HUI Zheng, et al. Study on law of longitudinal wave velocity evolution of dry hot rock after thermal shock[J]. Coal Science and Technology, 2021, 49(10): 58–65.

[21] PAI N, FENG J, HAIJIAN S, et al. An investigation on the deterioration of physical and mechanical properties of granite after cyclic thermal shock[J]. Geothermics, 2021, 97: 102252.

[22] ZHOU X P, ZHANG J Z, QIAN Q H, et al. Experimental investigation of progressive cracking processes in granite under uniaxial loading using digital imaging and AE techniques[J]. Journal of Structural Geology, 2019, 126: 129–145.

[23] LI M, LIU X S. Experimental and numerical investigation of the failure mechanism and permeability evolution of sandstone based on hydro-mechanical coupling[J]. Journal of Natural Gas Science and Engineering, 2021, 95: 104240.

[24] HOU C, JIN X, HE J, et al. Experimental studies on the pore structure and mechanical properties of anhydrite rock under freeze-thaw cycles[J]. Journal of Rock Mechanics and Geotechnical Engineering, 2022, 14(3): 781–797.

[25] LIU Quan-sheng, XU Xi-chang. Damage analysis of brittle rock at high temperature[J]. Chinese Journal of Rock Mechanics and Engineering, 2000, 19(4): 408–411.

[26] TANG Shi-bin, LUO Jiang, TANG Chun'an. Theoretical and numerical study on the cryogenic fracturing in rock[J]. Chinese Journal of Rock Mechanics and Engineering, 2018, 37(7): 1596–1607.

[27] ZHU Z, RANJITH P G, TIAN H, et al. Relationships between P-wave velocity and mechanical properties of granite after exposure to different cyclic heating and water cooling treatments[J]. Renewable Energy, 2021, 168: 375–392.

[28] WANG G, SUN F, WANG R, et al. Simulation of cryogenic fracturing of rock-like materials using material point method[J]. Journal of Natural Gas Science and Engineering, 2021, 96: 104300.

[29] XI Bao-ping, WU Yang-chun, WANG Shuai, et al. Experimental study on mechanical properties of granite taken from Gonghe basin, Qinghai province after high temperature thermal damage[J]. Chinese Journal of Rock Mechanics and Engineering, 2020, 39(1): 69–83.

[30] LI M, LIU X, PAN Y, et al. Experimental studies on the effect of cyclic thermal shock and cooling methods on the mechanical properties and fracture behavior of prefabricated fissured sandstone[J]. Theoretical and Applied Fracture Mechanics, 2022, 122: 103576.